EXOPLANETS

GJ 367b: A dense, ultrashort-period sub-Earth planet transiting a nearby red dwarf star

Kristine W. F. Lam[1,2]*†, Szilárd Csizmadia[2]†, Nicola Astudillo-Defru[3], Xavier Bonfils[4], Davide Gandolfi[5], Sebastiano Padovan[2,6], Massimiliano Esposito[7], Coel Hellier[8], Teruyuki Hirano[9]‡, John Livingston[10], Felipe Murgas[11,12], Alexis M. S. Smith[2], Karen A. Collins[13], Savita Mathur[11,12], Rafael A. Garcia[14,15], Steve B. Howell[16], Nuno C. Santos[17,18], Fei Dai[19], George R. Ricker[20], Roland Vanderspek[20], David W. Latham[13], Sara Seager[20,21,22], Joshua N. Winn[23], Jon M. Jenkins[16], Simon Albrecht[24], Jose M. Almenara[4], Etienne Artigau[4], Oscar Barragán[25], François Bouchy[26], Juan Cabrera[4], David Charbonneau[13], Priyanka Chaturvedi[7], Alexander Chaushev[1], Jessie L. Christiansen[27], William D. Cochran[28], José R. De Meideiros[29], Xavier Delfosse[4], Rodrigo F. Díaz[30], René Doyon[31], Philipp Eigmüller[2], Pedro Figueira[32,17], Thierry Forveille[4], Malcolm Fridlund[33,34], Guillaume Gaisné[4], Elisa Goffo[5,7], Iskra Georgieva[33], Sascha Grziwa[35], Eike Guenther[7], Artie P. Hatzes[7], Marshall C. Johnson[36], Petr Kabáth[37], Emil Knudstrup[24], Judith Korth[35,38], Pablo Lewin[39], Jack J. Lissauer[16,40], Christophe Lovis[26], Rafael Luque[11,12], Claudio Melo[32], Edward H. Morgan[20], Robert Morris[16,41], Michel Mayor[26], Norio Narita[42,43,44,11], Hannah L. M. Osborne[45], Enric Palle[11,12], Francesco Pepe[26], Carina M. Persson[33], Samuel N. Quinn[13], Heike Rauer[2,1,46], Seth Redfield[47], Joshua E. Schlieder[48], Damien Ségransan[26], Luisa M. Serrano[5], Jeffrey C. Smith[16,41], Ján Šubjak[37,49], Joseph D. Twicken[16,41], Stéphane Udry[26], Vincent Van Eylen[45], Michael Vezie[20]

Ultrashort-period (USP) exoplanets have orbital periods shorter than 1 day. Precise masses and radii of USP exoplanets could provide constraints on their unknown formation and evolution processes. We report the detection and characterization of the USP planet GJ 367b using high-precision photometry and radial velocity observations. GJ 367b orbits a bright (*V*-band magnitude of 10.2), nearby, and red (M-type) dwarf star every 7.7 hours. GJ 367b has a radius of 0.718 ± 0.054 Earth-radii and a mass of 0.546 ± 0.078 Earth-masses, making it a sub-Earth planet. The corresponding bulk density is 8.106 ± 2.165 grams per cubic centimeter—close to that of iron. An interior structure model predicts that the planet has an iron core radius fraction of 86 ± 5%, similar to that of Mercury's interior.

Red dwarf stars of spectral type M (M dwarfs) are cool stars with effective temperatures ($T_{\rm eff}$) below ~4000 K (*1*). They have masses and radii less than ~60% the size of those of the Sun and are the most abundant type of stars in the solar neighborhood (*2*–*4*). It has been estimated that M dwarfs host an average of 2.5 ± 0.2 small planets [planet radius $R_{\rm p} < 4$ Earth-radii ($R_\oplus$)] with periods <100 days (*5*). Because of the small stellar radius, the transit signal produced by a planet orbiting an M dwarf is larger than that of a planet of the same size orbiting a solar-type star (G dwarf). The radial velocity (RV) signal induced by a planet is also larger for an M dwarf host than for that of a G dwarf, as a result of the lower stellar mass. M dwarfs therefore provide an opportunity to search for exoplanets with a small radius and low mass. However, young M dwarfs often have high stellar activity, which gives rise to noise in the RV observations (*6*). RV analysis can be complicated even for old, inactive M dwarfs because their slow rotation periods have harmonics in the range of periods where small planets are sought (*7*).

GJ 367 (also cataloged as TOI-731) is an M dwarf located 9.41 pc from the Sun (*8*) with a brightness of 10.153 magnitudes in the optical *V* band and 5.78 magnitudes in the infrared *K* band. We observed this star with the High Accuracy Radial Velocity Planet Searcher (HARPS) spectrograph (*9*) and determined its stellar properties. GJ 367 has an effective temperature of $T_{\rm eff}$ = 3519 ± 70 K, a stellar mass $M_{\rm s}$ = 0.454 ± 0.011 solar masses ($M_\odot$), a stellar radius $R_{\rm s}$ = 0.457 ± 0.013 solar radii ($R_\odot$), and a stellar luminosity $L_{\rm s}$ = 0.0288 ± 00029 solar luminosities ($L_\odot$) (*9*) (Table 1).

The Transiting Exoplanet Survey Satellite (TESS) (*10*) observed GJ 367 during sector 9 of its survey. TESS acquired optical photometry at 2-min cadence for 27 days from 28 February 2019 to 26 March 2019. The light curve (brightness as a function of time) was extracted using the Science Processing Operations Center (SPOC) pipeline (*11*). This revealed a planet candidate with an orbital period of 0.32 days and a radius of 0.75 $R_\oplus$, which was designated TOI-731.01 by the TESS Science Office on the basis of the SPOC transit search and data validation results. We also searched for transit signals using the Détection Spécialisée de Transits (DST) algorithm (*12*), which indicated a transit-like signal every 0.32 days

[1]Centre for Astronomy and Astrophysics, Technical University Berlin, 10585 Berlin, Germany. [2]Institute of Planetary Research, German Aerospace Center, 12489 Berlin, Germany. [3]Departamento de Matemática y Física Aplicadas, Universidad Católica de la Santísima Concepción, Concepción, Chile. [4]Université Grenoble Alpes, Centre national de la recherche scientifique, Institut de Planétologie et d'Astrophysique de Grenoble, F-38000 Grenoble, France. [5]Dipartimento di Fisica, Università degli Studi di Torino, I-10125, Torino, Italy. [6]WorkGroup Solutions GmbH at European Organisation for the Exploitation of Meteorological Satellites, 64295 Darmstadt, Germany. [7]Thüringer Landessternwarte Tautenburg, D-07778 Tautenberg, Germany. [8]Astrophysics Group, Keele University, Staffordshire, ST5 5BG, UK. [9]Department of Earth and Planetary Sciences, Tokyo Institute of Technology, Tokyo, Japan. [10]Department of Astronomy, University of Tokyo, Tokyo, Japan. [11]Instituto de Astrofísica de Canarias, 38205 La Laguna, Tenerife, Spain. [12]Departamento de Astrofísica, Universidad de La Laguna, 38206 La Laguna, Tenerife, Spain. [13]Center for Astrophysics, Harvard and Smithsonian, Cambridge, MA, USA. [14]Institut de Recherche sur les Lois Fondamentales de l'Universe, Commissariat à l'Énergie Atomique et aux énergies alternatives, Université Paris-Saclay, F-91191 Gif-sur-Yvette, France. [15]Astrophysique, Instrumentation et modélisation, Commissariat à l'Énergie Atomique et aux énergies alternatives, Centre National de la recherche scientifique, Université Paris-Saclay, Université Paris Diderot, Sorbonne Paris Cité, F-91191 Gif-sur-Yvette, France. [16]NASA Ames Research Center, Moffett Field, CA, USA. [17]Instituto de Astrofísica e Ciênciasdo Espaço, Universidade do Porto, Centro de Astrofísica da Universidade do Porto, 4150-762 Porto, Portugal. [18]Departamento de Física e Astronomia, Faculdade de Ciências, Universidade do Porto, 4169-007 Porto, Portugal. [19]Division of Geological and Planetary Sciences, California Institute of Technology, Pasadena, CA, USA. [20]Department of Physics and Kavli Institute for Astrophysics and Space Research, Massachusetts Institute of Technology, Cambridge, MA, USA. [21]Department of Earth, Atmospheric and Planetary Sciences, Massachusetts Institute of Technology, Cambridge, MA, USA. [22]Department of Aeronautics and Astronautics, Massachusetts Institute of Technology, Cambridge, MA, USA. [23]Department of Astrophysical Sciences, Princeton University, Princeton, NJ, USA. [24]Stellar Astrophysics Centre, Department of Physics and Astronomy, Aarhus University, DK-8000 Aarhus C, Denmark. [25]Subdepartment of Astrophysics, Department of Physics, University of Oxford, Oxford, OX1 3RH, UK. [26]Geneva Observatory, University of Geneva, 1290 Versoix, Switzerland. [27]Infrared Processing and Analysis Center, Caltech, Pasadena, CA, USA. [28]Center for Planetary Systems Habitability and McDonald Observatory, The University of Texas, Austin, TX, USA. [29]Departamento de Física, Universidade Federal do Rio Grande do Norte, 59072-970 Natal, RN, Brazil. [30]International Center for Advanced Studies and Instituto de Ciencias Físicas (Consejo Nacional de Investigaciones Científicas y Técnicas), Escuela de Ciencia y Tecnología - Universidad Nacional de San Martín, Campus Miguelete, Buenos Aires, Argentina. [31]Institut de Recherche sur les Exoplantes, Dpartement de Physique, Universit de Montral, Montral, QC, H3C 3J7, Canada. [32]European Southern Observatory, Vitacura, Santiago, Chile. [33]Department of Space, Earth and Environment, Chalmers University of Technology, Onsala Space Observatory, 439 92 Onsala, Sweden. [34]Leiden Observatory, University of Leiden, 2300 RA, Leiden, Netherlands. [35]Rheinisches Institut für Umweltforschung an der Universität zu Köln, D-50931 Köln, Germany. [36]Las Cumbres Observatory, Goleta, CA, USA. [37]Astronomical Institute, Czech Academy of Sciences, 25165 Ondřejov, Czech Republic. [38]Department of Space, Earth and Environment, Astronomy and Plasma Physics, Chalmers University of Technology, 412 96 Gothenburg, Sweden. [39]The Maury Lewin Astronomical Observatory, Glendora, CA, USA. [40]Geological Sciences Department, Stanford University, CA, USA. [41]Search for Extraterrestrial Intelligence Institute, Mountain View, CA, USA. [42]Komaba Institute for Science, The University of Tokyo, Tokyo, Japan. [43]Japan Science and Technology Agency, Precursory Research for Embryonic Science and Technology, Tokyo, Japan. [44]Astrobiology Center, Tokyo, Japan. [45]Mullard Space Science Laboratory, University College London, Dorking, Surrey, RH5 6NT, UK. [46]Institute of Geological Sciences, Freie Universität Berlin, D-12249 Berlin, Germany. [47]Astronomy Department and Van Vleck Observatory, Wesleyan University, Middletown, CT, USA. [48]NASA Goddard Space Flight Center, Greenbelt, MD, USA. [49]Astronomical Institute of Charles University, 180 00 Prague, Czech Republic.
***Corresponding author. Email: kristine.lam@dlr.de** †These authors contributed equally to this work. ‡Present address: Astrobiology Center, 2-21-1 Osawa, Mitaka, Tokyo, Japan.

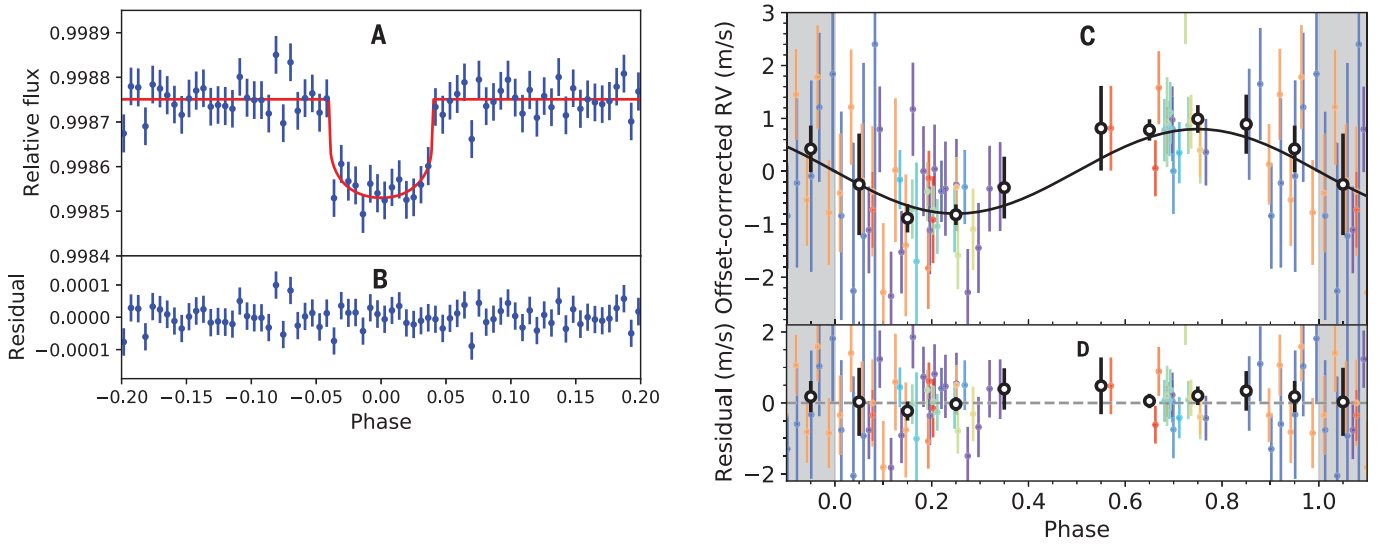

Fig. 1. Phase-folded RV and light curve of GJ 367. (**A**) Phase-folded, 2.6-min binned TESS light curve (blue circles) of GJ 367 with the best-fitting transit model (red line). Error bars show the 1-sigma uncertainties of the binned values. (**B**) The residuals of the light curve. A noise-correction model has been applied to the data (*9*). (**C**) Phase-folded HARPS RV data for GJ 367. Different color dots correspond to different corrections applied to the RV model (*9*). Black open circles are the RV data phase-binned in intervals of 0.10. The solid black line shows the best-fitting RV model, which has a semiamplitude of 79.8 ± 11.0 cm s^{-1}. (**D**) The corresponding residuals of the RV data. In (C) and (D), the RV orbital phase limits extend beyond phases 0 to 1 (shaded gray regions), so the first and last data points are duplicated.

and a transit depth of ~0.03%, corresponding to the transit of a sub-Earth–sized planet (Fig. 1).

We performed several tests to ensure that the candidate was not a false positive. Comparison of photometric data using varying aperture sizes showed no correlation between the aperture size and transit depth, indicating that the transit signal is not from another source blended with GJ 367. We performed follow-up ground-based photometry and found no contamination from eclipsing binaries up to 2.5 arc sec from the target star (*9*). The follow-up photometry shows that nearby stellar sources contribute 9.5 ± 1.2% of the flux within the TESS optimal aperture. This contamination reduces the transit depth, causing analysis of the TESS light curve to underestimate the planet's radius by ~5% (*9*). We account for this dilution factor in a transit model to obtain the true planet radius (Table 1). The density of the host star, ρ_s, was derived from the transit light curve (*9*), finding 7.64 ± 3.51 g cm^{-3}, which is consistent with the value $\rho_s = 6.71^{+0.61}_{-0.55}$ g cm^{-3} determined from the spectral analysis discussed above (*9*).

In a further test, we performed a frequency analysis of the HARPS RV measurements and stellar activity indicators (*9*). The periodogram of the RVs has a peak at orbital frequency (*f*) of 3.103 d^{-1} (*P* = 0.322 days) that has no counterpart in the periodograms of the activity indicators (fig. S4), consistent with a planetary origin. A further 45-day signal is present in the RV periodogram and in the activity indicators. Our analysis of archival photometry from the Wide Angle Search for Planets (WASP) survey indicates a stellar rotational period of 48 ± 2 days (*9*). GJ 367's Ca(II) activity index is log R'_{HK} = −5.214 ± 0.074, which corresponds to an estimated stellar rotation period of 58.0 ± 6.9 days (*9*). This indicates that the 45-day signal likely originates from active regions on the stellar surface. We conclude that the 0.322-day period is the result of an ultrashort-period (USP) planet, GJ 367b.

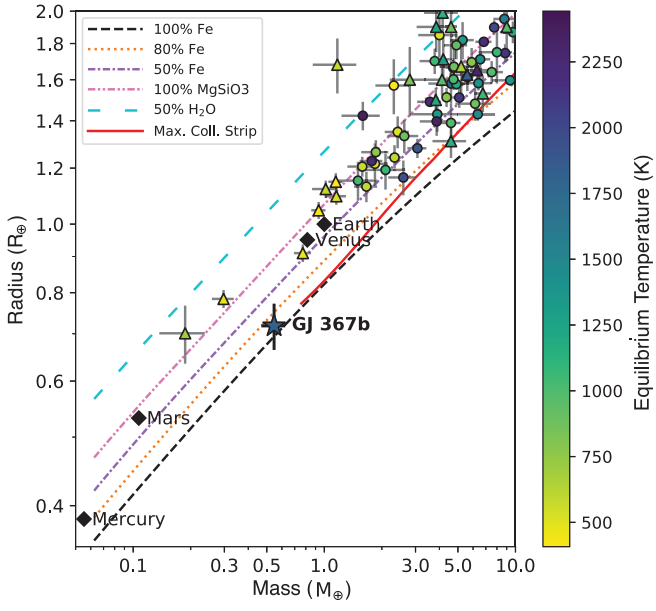

Fig. 2. Masses and radii of small planets (<2 $R_\oplus$) that have both quantities measured with precision ≤30%. Symbols indicate masses determined with RVs (circles) and transit timing variations (triangles), Solar System planets (diamonds), and GJ 367b (star). Error bars show 1-sigma uncertainties. Exoplanet symbols are color coded according to the equilibrium dayside temperatures (color bar). Theoretical mass-radius relations for two-layer rocky planets (*22*) are shown with lines corresponding to different core mass fractions. These cores consist of pure iron, pure rock (100% MgSiO3), or a two-layer core with a mixture of iron and rock or rock and H_2O ice, as indicated in the legend. The solid red line denotes the lower limit on planet radius after collisional stripping (*31*). GJ 367b is likely an iron-dominated planet.

Using a priori information on the host star properties from our spectral analysis, we derived the physical properties of the GJ 367 system using a Bayesian Markov chain Monte Carlo (MCMC) code, Transit and Light Curve Modeller (*13*), to model the transit photometry

Table 1. Properties of host star GJ 367 and planet GJ 367b. The stellar parameters were derived from the spectral analysis of the HARPS data (*9*). Planet parameters were obtained from the joint model fitting of the TESS photometry and HARPS RVs (*9*). Reported values are the medians of the posterior probability distributions with uncertainties of the 34th and 68th percentiles of those distributions.

Parameter	Value
Star GJ 367 (TOI 731)	
Right ascension (J2000 equinox)	$09^h44^m29.84^s$
Declination (J2000 equinox)	−45°46′35.43″
TESS-band magnitude	8.032 ± 0.007
V-band magnitude	10.153 ± 0.044
Parallax* (milli–arc sec)	106.272 ± 0.056
Distance, *d* (pc)	9.410 ± 0.005
Effective temperature, T_{eff} (K)	3522 ± 70
Stellar mass, M_s ($M_\odot$)	0.454 ± 0.011
Stellar radius, R_s ($R_\odot$)	0.457 ± 0.013
Stellar density, ρ_s ($\rho_\odot$)	$4.76^{+0.43}_{-0.39}$
Metallicity, [Fe/H]	−0.01 ± 0.12
Surface gravity, log *g*	4.777 ± 0.026
Luminosity, L_s ($L_\odot$)	0.0288 ± 0.0027
Spectral type	M1.0V
Planet GJ 367b	
Epoch, T_0 [barycentric Julian date (BJD_{TDB})]	2458544.1348 ± 0.0004
Orbital period, *P* (days)	$0.321962^{+0.000010}_{-0.000012}$
Planet-to-star radius ratio, R_p/R_s	$0.0143^{+0.0096}_{-0.0010}$
Scaled orbital semimajor axis, a/R_s	$3.41^{+0.06}_{-0.07}$
Impact parameter, *b*	$0.55^{+0.03}_{-0.04}$
RV semiamplitude†, *K* (cm s^{-1})	79.8 ± 11.0
Systemic RV‡, v_γ (km s^{-1})	47.9258 ± 0.0003
Eccentricity, *e*	0
Transit duration, T_{14} (min)	$36.9^{+1.0}_{-0.9}$
Orbital semimajor axis, *a* (astronomical units)	0.0071 ± 0.0002
Orbital inclination, *i* (°)	80.75 ± 0.64
Planet mass, M_p ($M_\oplus$)	0.546 ± 0.078
Planet radius, R_p ($R_\oplus$)	0.718 ± 0.054
Planet bulk density, ρ_p (g cm^{-3})	8.106 ± 2.165
Equilibrium dayside temperature§, assuming an Earth-like bond albedo (A_b = 0.3), T_{eq} (K)	1597 ± 39
Equilibrium dayside temperature§, assuming zero bond albedo, T_{eq} (K)	1745 ± 43

*A correction of +61 milli–arc sec was applied to the Gaia parallax (*9*). †RV induced by the orbiting planet. ‡RV of the star-planet system with respect to the observer. The uncertainty only reflects the internal precision of HARPS and does not account for systematic effects, such as gravitational redshift. §Assuming no atmospheric circulation.

and RV data simultaneously (*9*). Table 1 reports the physical properties of the planetary system from this analysis. The transit depth of 212 ± 42 parts per million (ppm) and RV semiamplitude K = 79.8 ± 11.0 cm s^{-1} correspond to a planetary radius of 0.718 ± 0.054 $R_\oplus$ and a planetary mass of 0.546 ± 0.078 Earth-masses ($M_\oplus$). Figure 1 shows the phase-folded light curve and RV measurements of GJ 367 along with the corresponding best-fitting transit and RV models. We find that GJ 367b is a sub-Earth planet with a high expected signal-to-noise metric for emission spectroscopy (see supplementary text). The planet receives high stellar irradiation because of its close proximity to the host star, ~576 times the incident flux on Earth. This corresponds to a dayside temperature of 1745 ± 43 K (assuming zero Bond albedo), which is high enough to evaporate any primordial atmosphere (*14*–*16*) and begin to melt or vaporize any silicates or metallic iron (*17*).

The measured mass and radius of GJ 367b imply a bulk density of 8.106 ± 2.165 g cm^{-3}. The bulk composition of a planet can be estimated from theoretical mass-radius relations (*18*–*21*). Figure 2 shows the mass and radius distribution of small planets (R_p below 2 $R_\oplus$) along with theoretical predictions for rocky planets (*21*, *22*). GJ 367b has a mass and radius consistent with an interior dominated by an iron core. This is similar to two larger USP planets, K2-229b (*23*) and K2-141b (*24*, *25*), which have enhanced iron fractions (Fig. 3A). Other known planets with similar sizes to GJ 367b, such as Kepler-138 b (*26*, *27*) and TRAPPIST-1 d (*28*, *29*), have lower densities and longer orbital periods and are exposed to lower stellar irradiation, so they may be less susceptible to loss of an atmosphere (*14*).

We used a neural network to investigate possible interior structures of GJ 367b (*9*). At the best-fitting density, the neural network indicates that GJ 367b is predominantly made of iron (Fig. 3B), composed of 86 ± 5% iron core (by radius), <10% water ice and/or a H and He gas envelope, and the remainder as silicate mantle. This composition is similar to that of Mercury, which the neural network predicts would have an iron core radius fraction of 81 ± 4% (*9*). This is consistent with the measured Mercury core radius of 2030 ± 37 km (*30*), which corresponds to a core radius fraction of 83 ± 2%. For comparison, the interior structures of Mercury and other terrestrial planets predicted by our analysis are shown in fig. S8.

REFERENCES AND NOTES

1. C. Cifuentes *et al.*, *Astron. Astrophys.* **642**, A115 (2020).

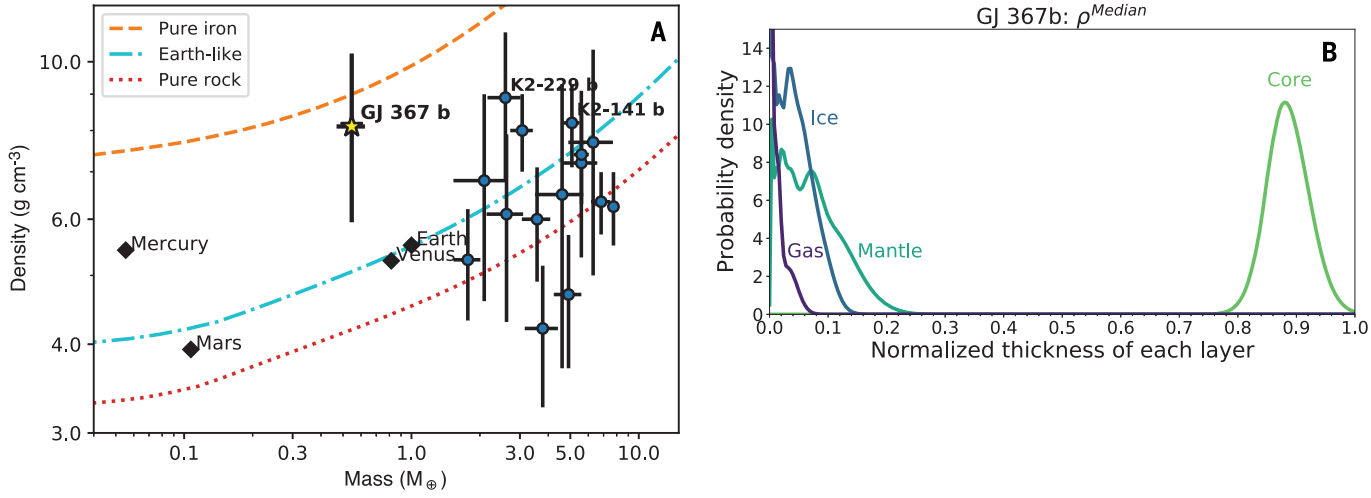

Fig. 3. Bulk composition of USP planets and predicted interior structure of GJ 367b. (**A**) Mass-density diagram for USP (P_{orb} < 1 day) exoplanets with low mass (<10 $M_{\oplus}$) and measured mass precisions ≤30%. Inner Solar System planets are shown as black diamonds. Planet interior composition models (*22*) are shown with lines indicated in the legend. The bulk densities of low-mass USP planets are usually consistent with terrestrial compositions (pure rock or Earth-like). GJ 367b is more consistent with pure iron and an interior similar to that of Mercury. (**B**) The predicted relative thicknesses of each interior layer of GJ 367b from the neural network model (*32*). The core is assumed to be a liquid Fe-FeS alloy. The mantle is assumed to be composed of olivine and orthopyroxene enstatite in the upper mantle and bridgmanite and magnesiowüstite in the lower mantle. The ice layer is assumed to be water ice VII, and the gas layer consists of hydrogen and helium. The interior composition of GJ 367b was computed using the median mass and radius measurements (corresponding to the derived median planet density ρ^{Median} = 8.106 g cm^{-1}). We infer an iron core filling 86 ± 5% of the planet radius with <1% ice and gas, similar to the interior of Mercury, which has an iron core radius fraction of 83 ± 2% (*30*). If we take the lowest density of GJ 367b permitted by the observations, 5.941 g cm^{-1}, the planet iron core radius fraction is still higher than that of Earth (fig. S7).

2. E. E. Salpeter, *Astrophys. J.* **121**, 161 (1955).
3. T. J. Henry *et al.*, *Astron. J.* **132**, 2360–2371 (2006).
4. G. Chabrier, *Publ. Astron. Soc. Pac.* **115**, 763–795 (2003).
5. C. D. Dressing, D. Charbonneau, *Astrophys. J.* **807**, 45 (2015).
6. A. Suárez Mascareño *et al.*, *Astron. Astrophys.* **639**, A77 (2020).
7. S. H. Saar, R. A. Donahue, *Astrophys. J.* **485**, 319–327 (1997).
8. A. G. A. Brown *et al.*, *Astron. Astrophys.* **616**, A1 (2018).
9. Materials and methods are available as supplementary materials.
10. G. R. Ricker *et al.*, in *Space Telescopes and Instrumentation 2016: Optical, Infrared, and Millimeter Wave*, H. A. MacEwen *et al.*, Eds., vol. 9904 of *Society of Photo-Optical Instrumentation Engineers (SPIE) Proceedings* (2016), pp. 99042B.
11. J. M. Jenkins *et al.*, in *Software and Cyberinfrastructure for Astronomy IV*, G. Chiozzi, J. C. Guzman, Eds., vol. 9913 of *SPIE Proceedings* (2016), pp. 99133E.
12. J. Cabrera, S. Csizmadia, A. Erikson, H. Rauer, S. Kirste, *Astron. Astrophys.* **548**, A44 (2012).
13. S. Csizmadia, *Mon. Not. R. Astron. Soc.* **496**, 4442–4467 (2020).
14. J. E. Owen, Y. Wu, *Astrophys. J.* **847**, 29 (2017).
15. E. D. Lopez, J. J. Fortney, *Astrophys. J.* **792**, 1 (2014).
16. J. E. Owen, Y. Wu, *Astrophys. J.* **775**, 105 (2013).
17. A. Léger *et al.*, *Icarus* **213**, 1–11 (2011).
18. D. Valencia, D. D. Sasselov, R. J. O'Connell, *Astrophys. J.* **665**, 1413–1420 (2007).
19. L. Zeng, D. Sasselov, *Publ. Astron. Soc. Pac.* **125**, 227–239 (2013).
20. S. Seager, M. Kuchner, C. A. Hier-Majumder, B. Militzer, *Astrophys. J.* **669**, 1279–1297 (2007).
21. L. Zeng, D. D. Sasselov, S. B. Jacobsen, *Astrophys. J.* **819**, 127 (2016).
22. L. Zeng *et al.*, *Proc. Natl. Acad. Sci. U.S.A.* **116**, 9723–9728 (2019).
23. A. Santerne *et al.*, *Nat. Astron.* **2**, 393–400 (2018).
24. O. Barragán *et al.*, *Astron. Astrophys.* **612**, A95 (2018).
25. L. Malavolta *et al.*, *Astron. J.* **155**, 107 (2018).
26. D. Jontof-Hutter, J. F. Rowe, J. J. Lissauer, D. C. Fabrycky, E. B. Ford, *Nature* **522**, 321–323 (2015).
27. J. M. Almenara, R. F. Díaz, C. Dorn, X. Bonfils, S. Udry, *Mon. Not. R. Astron. Soc.* **478**, 460–486 (2018).
28. M. Gillon *et al.*, *Nature* **533**, 221–224 (2016).
29. M. Gillon *et al.*, *Nature* **542**, 456–460 (2017).
30. D. E. Smith *et al.*, *Science* **336**, 214–217 (2012).
31. R. A. Marcus, D. Sasselov, L. Hernquist, S. T. Stewart, *Astrophys. J. Lett.* **712**, L73–L76 (2010).
32. P. Baumeister *et al.*, *Astrophys. J.* **889**, 42 (2020).

ACKNOWLEDGMENTS

We acknowledge use of observations from the LCOGT network. We made use of data from the European Space Agency (ESA) mission Gaia (www.cosmos.esa.int/gaia), processed by the Gaia Data Processing and Analysis Consortium (DPAC) (www.cosmos.esa.int/web/gaia/dpac/consortium). Funding for DPAC has been provided by national institutions, in particular the institutions participating in the Gaia Multilateral Agreement. We acknowledge the use of public TESS Alert data from pipelines at the TESS Science Office and at the TESS Science Processing Operations Center. This work was supported by the KESPRINT collaboration, an international consortium devoted to the characterization and research of exoplanets discovered with space-based missions. Some of the observations were made at Gemini South using the high-resolution imaging instrument Zorro, funded by the NASA Exoplanet Exploration Program and built at the NASA Ames Research Center by S. B. Howell, N. Scott, E. P. Horch, and E. Quigley. Zorro was mounted on the Gemini South telescope of the international Gemini Observatory, a program of NSF's OIR Lab, which is managed by the Association of Universities for Research in Astronomy (AURA) under a cooperative agreement with the National Science Foundation on behalf of the Gemini partnership: the National Science Foundation (United States); the National Research Council (Canada); Agencia Nacional de Investigacin y Desarrollo (Chile); Ministerio de Ciencia, Tecnologa e Innovacin (Argentina); Ministrio da Ciência, Tecnologia, Inovaes e Comunicaes (Brazil); and the Korea Astronomy and Space Science Institute (Republic of Korea). This is University of Texas Center for Planetary Systems Habitability Contribution no. 0041. **Funding:** K.W.F.L., Sz.Cs., M.E., S.G., A.P.H., and H.R. were supported by Deutsche Forschungsgemeinschaft grants PA525/18-1, PA525/19-1, PA525/20-1, HA3279/12-1, and RA714/14-1 within the DFG Schwerpunkt SPP 1992, Exploring the Diversity of Extrasolar Planets. Sz.Cs. is supported by Deutsche Forschungsgemeinschaft Research Unit 2440, Matter Under Planetary Interior Conditions: High Pressure Planetary and Plasma Physics. T.H. was supported by JSPS KAKENHI grant no. JP19K14783, and N.N. was supported by JSPS KAKENHI grant nos. JP18H01265 and JP18H05439 and JST PRESTO grant no. JPMJPR1775. J.L. is supported by JSPS KAKENHI grant no. JP20K14518. R.A.G. acknowledges support from PLATO and GOLF CNES grants. P.K. acknowledges support from the MSMT grant LTT20015. S.M. acknowledges support by the Spanish Ministry of Science and Innovation with the Ramon y Cajal fellowship no. RYC-2015-17697 and grant no. PID2019-107187GB-I00. N.C.S. was supported by Fundaçao para a Ciência e a Tecnologia through national funds and by FEDER through COMPETE2020 - Programa Operacional Competitividade e Internacionalização grants UID/FIS/04434/2019, UIDB/04434/2020, UIDP/04434/2020, PTDC/FIS-AST/32113/2017 and POCI-01-0145-FEDER-032113, and PTDC/FIS-AST/28953/2017 and POCI-01-0145-FEDER-028953. X.D. and G.G. acknowledge funding in the framework of the Investissements d'Avenir program (ANR-15-IDEX-02), Origin of Life project of the Université Grenoble-Alpes. J.R.D.M. acknowledges grants from CNPq, CAPES, and FAPERN Brazilian agencies. N.A.-D. acknowledges support from FONDECYT project 3180063. Resources for the production of the SPOC data products were provided by the NASA High-End Computing (HEC) program through the NASA Advanced Supercomputing (NAS) Division at Ames Research Center. S.A. is supported by the Danish National Research Foundation (grant agreement no. DNRF106). D.G. and L.M.S. acknowledge financial support from the Cassa di Risparmio di Torino foundation under grant no. 2018.2323, "Gaseous or rocky? Unveiling the nature of small worlds." **Author contributions:** K.W.F.L. contributed to the planet detection, transit light curve analysis, gyrochronology age estimate, and tidal evolution calculations and led the writing of the paper. Sz.Cs. performed the joint light curve and RV analysis using the Transit and Light Curve Modeller (TLCM). N.A.-D. and X.B. led the HARPS RV follow-up program and reduced and analyzed the RV data. D.G. performed the frequency analysis of the RV and activity indicators. F.D., O.B., A.P.H., and R.L. analyzed the RV data. S.P. determined the interior composition of the planet and modeled the precursor gaseous planet. M.E. performed the Rapid Eye Mount (REM) robotic telescope observations and analysis. M.E. and A.M.S.S. derived the light curve dilution factor. C.H., K.W.F.L., S.M., and R.A.G. determined the stellar rotation period using WASP data. S.B.H. analyzed the speckle imaging data. T.H. and M.F. performed the spectral analysis using SpecMatch-Emp, and T.H. derived the stellar parameters using an MCMC simulation. J.L. performed stellar characterization using isochrone fitting. F.M. performed the LCOGT and HARPS observations. K.A.C. coordinated the TESS SG1 working group. K.A.C. and P.L. analyzed the ground-based photometric observations. N.C.S. performed spectral characterization using ODUSSEAS. M.C.J. determined the Galactic space velocities of the star. K.W.F.L. and S.R. calculated the emission spectroscopy metric. J.K. performed transit-timing variation (TTV) analysis. J.C., P.E., and S.G. analyzed the

light curve for planet detection. E.Gu. analyzed the activity indicators. G.R.R., R.V., D.W.L., S.S., J.N.W., and J.M.J. led and organized the TESS mission, including the observations, processing of the data, working groups coordination, target selection, and dissemination of the data products. E.H.M., M.V., and J.E.S. are members of the TESS POC who coordinated and scheduled the TESS science observations and conducted instrument planning. R.M., J.C.S., and J.D.T. are members of the SPOC who performed data calibration, light curve production, and transit planet detection. D.C., J.C., and S.N.Q. are members of the TSO who reviewed the data and performed planet candidate vetting. J.M.A., E.A., F.B., D.C., J.R.D.M., X.D., R.F.D., R.D., P.F., T.F., G.G., C.L., C.M., F.P., D.S., and S.U. are coinvestigators of the proposal, which provided the HARPS observations of the target and supported the interpretation of results. S.A., P.C., A.C., W.D.C., E.Go., I.G., P.K., E.K., J.J.L., N.N., H.L.M.O., E.P., C.M.P., H.R., L.M.S., J.Š., and V.V.E. are part of the KESPRINT consortium and contributed to the interpretation of the results. All authors contributed to the preparation of the paper.

Competing interests: The authors declare no competing interests.

Data and materials availability: The TESS photometric observations are available at the Mikulski Archive for Space Telescopes (MAST) at https://exo.mast.stsci.edu under target name TOI 731.01. The raw HARPS spectroscopic data are available on the ESO Science Archive Facility http://archive.eso.org/cms.html under ESO program IDs 072.C-0488, 082.C-0718, 183.C-0437 (primary investigators: M. Mayor and X. Bonfils), and 1102.C-0339 (primary investigator: X. Bonfils). The ground-based photometry obtained by the LCO telescope and REM as well as the Gemini imaging data are available on the Exoplanet Follow-up Observing Program (ExoFOP) website https://exofop.ipac.caltech.edu/tess/ under target name TOI 731.01. The raw Gemini data are available at https://archive.gemini.edu/searchform under program ID GS-2021A-LP-105. The archival WASP data are available on the NASA Exoplanet Archive https://exoplanetarchive.ipac.caltech.edu/docs/SuperWASPMission.html under object name GJ 367. Our reduced RVs and activity indices are listed in tables S1 and S2 and in machine-readable form in data S1 and S2. The TLCM is available at www.transits.hu/.

SUPPLEMENTARY MATERIALS

science.org/doi/10.1126/science.aay3253
Materials and Methods
Supplementary Text
Figs. S1 to S10
Tables S1 to S3
References (*33*–*127*)
Data S1 and S2

31 December 2020; accepted 12 October 2021
10.1126/science.aay3253

Science

GJ 367b: A dense, ultrashort-period sub-Earth planet transiting a nearby red dwarf star

Kristine W. F. LamSzilárd CsizmadiaNicola Astudillo-DefruXavier BonfilsDavide GandolfiSebastiano PadovanMassimiliano EspositoCoel HellierTeruyuki HiranoJohn LivingstonFelipe MurgasAlexis M. S. SmithKaren A. CollinsSavita MathurRafael A. GarciaSteve B. HowellNuno C. SantosFei DaiGeorge R. RickerRoland VanderspekDavid W. LathamSara SeagerJoshua N. WinnJon M. JenkinsSimon AlbrechtJose M. AlmenaraEtienne ArtigauOscar BarragánFrançois BouchyJuan CabreraDavid CharbonneauPriyanka ChaturvediAlexander ChaushevJessie L. ChristiansenWilliam D. CochranJosé R. De MeideirosXavier DelfosseRodrigo F. DíazRené DoyonPhilipp EigmüllerPedro FigueiraThierry ForveilleMalcolm FridlundGuillaume GaisnéElisa GoffoIskra GeorgievaSascha GrziwaEike GuentherArtie P. HatzesMarshall C. JohnsonPetr KabáthEmil KnudstrupJudith KorthPablo LewinJack J. LissauerChristophe LovisRafael LuqueClaudio MeloEdward H. MorganRobert MorrisMichel MayorNorio NaritaHannah L. M. OsborneEnric PalleFrancesco PepeCarina M. PerssonSamuel N. QuinnHeike RauerSeth RedfieldJoshua E. SchliederDamien SégransanLuisa M. SerranoJeffrey C. SmithJán ŠubjakJoseph D. TwickenStéphane UdryVincent Van EylenMichael Vezie

Science, 374 (6572), • DOI: 10.1126/science.aay3253

A nearby iron-rich sub-Earth planet

The mass and radius of an exoplanet determine its mean density, which provides information about the possible interior structure. Lam *et al*. have identified a planet on a 7.7-hour orbit around a nearby red dwarf star. The authors determined the planet's radius from the transit, then used radial velocity observations to measure the mass. They found a sub-Earth–sized planet with a density almost equivalent to pure iron. Its high surface temperature is close to the vaporization point of iron, suggesting that it is the iron core of a planet that has lost its outer mantle. —KTS

Science (ISSN) is published by the American Association for the Advancement of Science. 1200 New York Avenue NW, Washington, DC 20005. The title *Science* is a registered trademark of AAAS.